I&EC research
Industrial & Engineering Chemistry Research

Article

pubs.acs.org/IECR

Alumina with Various Pore Structures Prepared by Spray Pyrolysis of Inorganic Aluminum Precursors

Chang Liu,[†,‡] Yongchun Liu,[†] Qingxin Ma,[†] Jinzhu Ma,[†] and Hong He*[,†]

[†]Research Center for Eco-Environmental Sciences, Chinese Academy of Sciences, Beijing 100085, China

[‡]Chinese Academy of Meteorological Sciences, Beijing 100081, China

ABSTRACT: The microstructure of alumina plays a critical role in the catalytic performance of catalysts based on alumina; thus, the preparation of alumina with various pore structures has been the focus of great attention. In this study, alumina products with different microstructures were obtained from alumisol, $AlCl_3{\cdot}6H_2O$, and $Al(NO_3)_3{\cdot}9H_2O$ by the spray pyrolysis method. The pore structures of the alumina products were found to be closely related to the morphologies of aluminum precursors. The rod-shaped colloidal particles in the alumisol cross-linked with each other to form a mesoporous framework with cylinder pores. The lamellar-shaped $AlCl_3$ flakes overlapped during atomization and evaporation and subsequently led to the formation of lamellar pores. $Al(NO_3)_3$ underwent melting and decomposition during the spray pyrolysis process, resulting in the generation of solid particles. The present study also provides a flexible and economical opportunity for the industrial production of alumina with various microstructures.

1. INTRODUCTION

Alumina has abundant applications in the ceramics industry and heterogeneous catalysis and has been widely used as absorbents, abrasive materials, and biomaterials.[1−5] The application of alumina depends greatly on its properties, such as surface area, morphology, porosity, and so on. To fulfill the requirements in different fields, alumina with different surface areas (50−700 $m^2{\cdot}g^{-1}$), morphologies (e.g., spherical, nanorod, or irregular), particle sizes (nanometers to micrometers), phase compositions (γ, κ, θ, η, or α phase), and microstructures (e.g., mesoporous or microporous structure) can be produced.[1,6−8] Among these properties, the pore structure is one of the most important because most catalysts based on mesostructured alumina exhibit excellent catalytic activity.[9] For conventional alumina with uncontrolled porosity, deactivation could be induced by coking and plugging, consequently hindering the diffusion of reactants and products.[10,11] For instance, mesoporous alumina-supported Re_2O_7 catalysts give rise to a 3-fold higher conversion activity in the self-metathesis of 1-hexene than the same catalysts supported on γ-Al_2O_3 without a uniform pore structure.[12] As a result, the preparation of alumina with certain pore structures is of tremendous interest for both technological applications and fundamental research.

Commercial alumina is usually manufactured by the precipitation of aluminum salts,[13] sol−gel processing of aluminum alkoxides,[14,15] or powder processing technology using various inorganic or organic aluminum precursors.[16−18] Compared to other processes, spray pyrolysis is widely used in industry for the scalable preparation of powder materials because it is relatively inexpensive and quite versatile.[19−23] During the preparation process, atomized droplets of a precursor solution undergo evaporation and shrinkage while flowing through a high-temperature reactor and eventually form particles.[24−26] This method is therefore a continuous flow process and is more economical than other approaches (such as sol−gel processes) that involve multiple steps.[24,27] Through the spray method, alumina particles with different properties can be prepared by controlling the process parameters, such as precursor, residence time, and decomposition temperature.[4,28−30] For example, alumina particles with different morphologies (spherical, hollow, or doughnut-like) have been generated when various kinds of inorganic or metallo-organic alumina sources were used as precursor solutions.[30−34] Aside from the morphology, attention has also been paid to the adjustment of the microstructure, especially the preparation of mesoporous alumina with a uniform pore structure. For instance, mesoporous alumina can be prepared by the spray pyrolysis of $Al(NO_3)_2{\cdot}9H_2O$ in the presence of the surfactants cetyltrimethylammonium bromide (CTAB) and urea.[35] Additionally, Song et al.[8] prepared mesoporous alumina particles using spray pyrolysis by changing the types of organic surfactants and Al precursors. It should be noticed that the formation of mesostructures in these works was attributed to the use of structure-directing reagents. The obtained morphologies and structural properties (surface areas, pore volumes, pore size distributions) were strongly influenced by the templating agents.[8,35]

In our previous work, we synthesized mesoporous alumina with a uniform pore structure by alumisol spray pyrolysis without any structure-directing reagents.[36] The costs due to surfactants were effectively reduced, and the impurity problem caused by the incomplete decomposition of additives was also avoided. Furthermore, the results implied that the precursor itself might also play a critical role in the formation of microstructures. Therefore, in this work, we chose three inorganic alumina sources, namely, alumisol, $AlCl_3{\cdot}6H_2O$, and $Al(NO_3)_3{\cdot}9H_2O$, to study the effect of the precursor on the

Received: April 18, 2013
Revised: July 28, 2013
Accepted: August 27, 2013
Published: August 27, 2013

pore structure of alumina prepared by the spray pyrolysis method. The relationships between precursors and products were investigated, and a possible formation mechanism of different pore structures was proposed based on the results.

2. MATERIAL AND METHODS

2.1. Particle Synthesis. Boehmite-phase alumisol (AlOOH, lot no. 2205, Kawaken Fine Chemicals Co., Ltd.) and solutions of $AlCl_3 \cdot 6H_2O$ (AR, >99.0%, Sinopharm Chemical Reagent Co. Ltd.) and $Al(NO_3)_2 \cdot 9H_2O$ (AR, >99.0%, Sinopharm Chemical Reagent Co. Ltd.) were used as the precursors. The concentration of the precursors was 1.0 wt % calculated according to Al_2O_3 content. The pH values of alumisol, $Al(NO_3)_3$ solution, and $AlCl_3$ solution were measured to be 3.94, 3.71, and 2.56, respectively. The spray pyrolysis system and its instrumentation was described in detail elsewhere.[36] Briefly, it consists of a homemade atomizer, a diffusion dryer, and a corundum tube located inside a tubular furnace. Atomization of the liquid precursors was achieved by introducing synthetic air flow into the atomizer, and the sprayed precursor droplets were carried through the diffusion dryer to remove water. The partly dried droplets were then carried into the corundum tube embedded in the tubular furnace, and eventually, the powder product was collected by a filter sampler. The temperature of the tubular furnace was controlled at 1000 °C. The air flow rate was kept at 1.0 L·min^{-1}, corresponding to a residence time of 2.9 s.

2.2. Characterization of Prepared Particles. The crystalline structure of the products was determined by a powder X-ray diffraction (XRD) on a PANalytical X'Pert PRO X-ray powder diffractometer with Cu Kα radiation (λ = 0.154 nm) at 40 kV and 40 mA. The scan rate was 4° 2θ·min^{-1} from 10° to 90° 2θ. Peak positions and relative intensities were characterized by comparison with International Centre for Diffraction Data (ICDD) files.

The particle size distributions of the prepared alumina samples were measured online using a TSI 3936 scanning mobility particle sizer (SMPS). It consists of a TSI 3085 nano differential mobility analyzer (DMA) and a TSI 3025A condensation particle counter (CPC). The particle size data from the SMPS were taken over the size range from 20 to 1000 nm.

The surface areas and pore structures of the precursors and obtained products were measured using a Quantachrome Autosorb-1C-TCD analyzer by N_2 adsorption−desorption at −196 °C. The surface area (S_{BET}) was determined by applying the Brunauer−Emmett−Teller (BET) method to the adsorption isotherm in the range of 0.05−0.30, whereaas the pore volume (V_{BJH}), pore diameter (D_{BJH}), and pore size distribution were determined by the Barrett−Joyner−Halenda (BJH) equation from the desorption isotherm. The systematic errors of S_{BET}, V_{BJH}, and D_{BJH} determined by at least three tests for one sample were ±0.76%, ±1.1%, and ±0.03%, respectively.

The morphologies of precursors and products were characterized by transmission electron microscopy (TEM) using a Hitachi H-7500 apparatus operating at 40 kV. Precursor samples were collected directly onto Cu microgrids at the outlet of the atomizer. Product samples were ultrasonically dispersed in ultrapure water (18 MΩ), and a droplet of suspending liquid was deposited onto a Cu microgrid and allowed to dry.

3. RESULTS AND DISCUSSION

3.1. Crystallinity and Particle Size Distribution of Produced Alumina Particles. The X-ray diffraction spectra of products obtained from alumisol, $AlCl_3$, and $Al(NO_3)_3$ are displayed in Figure 1. The main peaks observed in the spectra

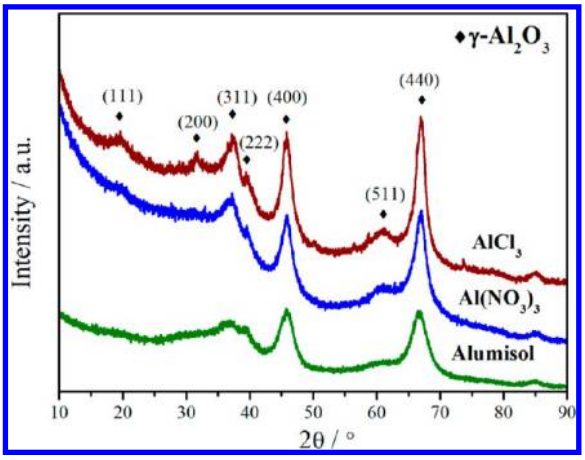

Figure 1. XRD patterns of products prepared from different precursors [$AlCl_3$, $Al(NO_3)_3$, and alumisol] at 1000 °C with a carrier air flow rate of 1.0 L·min^{-1}.

of the produced samples could be attributed to γ-Al_2O_3.[37] This indicates that γ-phase alumina was prepared from all of these precursors. The sharper diffraction peaks of products obtained from $AlCl_3$ and $Al(NO_3)_3$ implied that their crystallinities were much better than that of alumina prepared from alumisol. Alumina has various transition phases, including γ, δ, η, θ, β, κ, and α phases.[38] Generally, γ-Al_2O_3 appears at around 450 °C during the thermal decomposition of aluminum sol or salts, whereas the transformation from the η phase to θ-Al_2O_3 occurs at 1000 °C.[39] Although the preparation temperature used in this work was 1000 °C, the obtained alumina phase was the γ phase for all samples. Because the complete crystallization of the crystal phase requires continuous heat treatment at a certain temperature for several hours, the short residence time here might restrain complete crystallization. This is similar to our previous study in which the phase transformation temperature of alumina shifted to a higher range during the spray pyrolysis process.[36]

The particle size distributions of alumina prepared from different precursors were measured by SMPS. As illustrated in Figure 2, all alumina samples exhibited broad size distributions with particle sizes ranging from 100 to 500 nm. A broad size distribution is always observed when particles are produced by the spray method.[19] Compared to particles prepared from $AlCl_3$ and $Al(NO_3)_3$, alumina produced from alumisol had the largest particles. The agglomeration and coagulation of primary particles contribute to the growth of the particle size.[19,23] It has been reported that the interfacial force between primary particles formed in sol or solution will increase with increasing pH value, and then the aggregation will be enhanced.[40,41] This means that more agglomerate particles with larger diameters will be produced from solutions or sols with higher pH values. In the present study, more particles with larger sizes were prepared from alumisol. This might be because the pH value of alumisol (pH 3.94) is higher than those of $Al(NO_3)_3$ solution (pH 3.71) and $AlCl_3$ solution (pH 2.56).

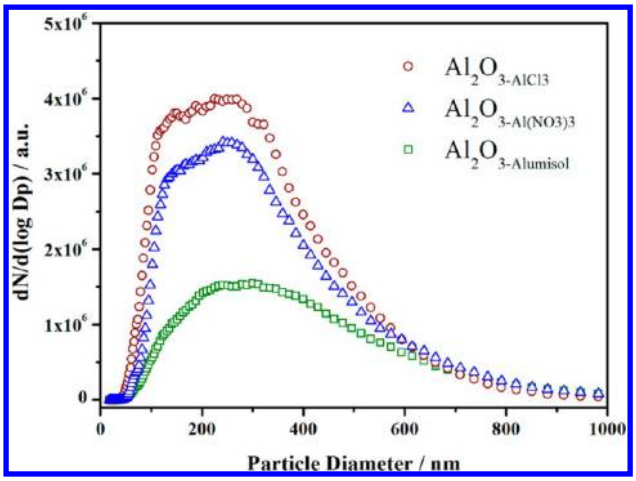

Figure 2. Particle size distributions of particles prepared from alumisol, $AlCl_3$, and $Al(NO_3)_3$ at 1000 °C with a carrier air flow rate of 1.0 L·min^{-1}.

3.2. Pore Structure of Prepared Alumina Particles. The porosities and surface areas of alumina samples were investigated by N_2 adsorption−desorption at −196 °C. Figure 3A shows that the types of hysteresis loops clearly varied with the precursors. Alumina prepared from alumisol presented an isotherm with an H2-type hysteresis loop, characteristic of a mesoporous structure with interconnected cylinder pore networks.[36,42,43] The sample prepared from $AlCl_3$ exhibited an H3-type hysteresis loop characteristic of mesoporous particles with a lamellar pore structure.[42] For the particles prepared from $Al(NO_3)_3$, however, no pore structure was exhibited.

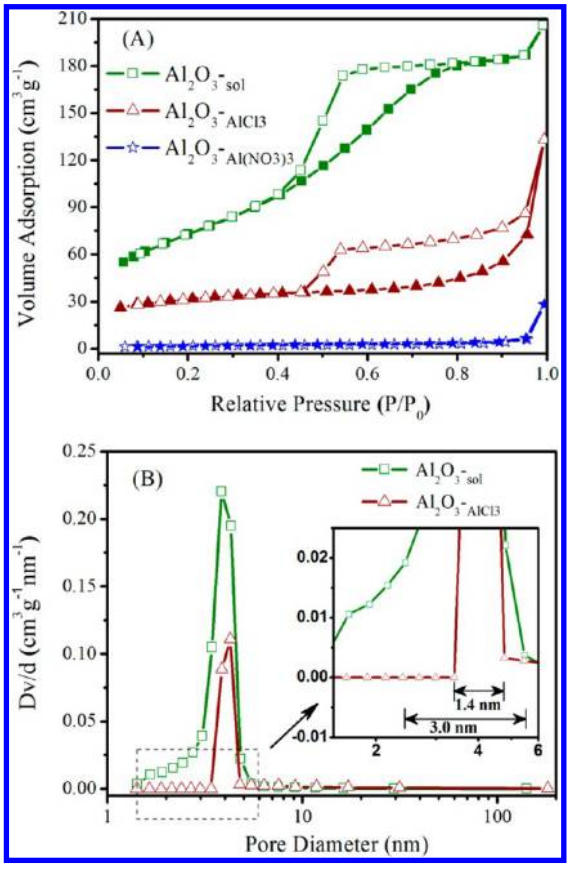

Figure 3. (A) Adsorption−desorption isotherms and (B) corresponding pore size distributions of samples prepared from different precursors at 1000 °C with a carrier air flow rate of 1.0 L·min^{-1}. Solid points in panel A denote adsorption data.

Figure 3B shows the pore size distributions obtained from the BJH method on the basis of the desorption data. Because there was no pore structure in the alumina prepared from $Al(NO_3)_3$, the pore size distributions of only the samples obtained from alumisol and $AlCl_3$ are compared in Figure 3B. This shows that the alumina obtained from both alumisol and $AlCl_3$ exhibited well-defined mesoporous structures with narrow pore size distributions. The pore size of alumina prepared from alumisol ranged from 2.5 to 5.5 nm, with the most probable pore size at approximately 3.8 nm. The alumina produced from $AlCl_3$ presented a much narrower pore size distribution (3.4−4.8 nm) with a most probable pore size at 4.3 nm. It has been demonstrated that the deactivation of the catalysts based on alumina is greatly aggravated by wider pore size distributions and additional micropores contributing to the specific surface area.[44] It should be noted that such a uniform mesoporous structure was obtained without the use of structure-directing reagents such as surfactants. This can avoid the surfactant removal step, which can cause the collapse of the mesoporous structure.[45] With a narrower pore size distribution and a more stable mesoporous structure, the as-prepared mesoporous alumina might have great application potential in catalysis.

The BET surface areas and pore structure parameters (volume and size) of the obtained alumina samples and corresponding precursors are summarized in Table 1. Alumina obtained from alumisol presented the largest surface area (284.5 m^2·g^{-1}) and pore volume (0.3597 cm^3·g^{-1}), whereas alumina prepared from $Al(NO_3)_3$ exhibited the smallest surface area (5.803 m^2·g^{-1}) and pore volume (0.0435 cm^3·g^{-1}). The small surface area and pore volume also indicated that the alumina obtained from $Al(NO_3)_3$ precursor was mainly solid particles. It is interesting to note that the S_{BET}, V_{BJH}, and D_{BJH} values of the obtained alumina were quite different from those of the $AlCl_3$ precursor. The values of the BET surface area, pore volume, and pore size of $AlCl_3$ were all very small (0.04604 m^2·g^{-1}, 0.0004457 cm^3·g^{-1}, and 1.412 nm, respectively), implying that there was no pore structure in $AlCl_3$ precursor particles. In contrast, the values of the BET surface area, pore volume, and pore size of the alumina obtained from $AlCl_3$ increased to 69.16 m^2·g^{-1}, 0.1884 cm^3·g^{-1}, and 4.269 nm, respectively. Therefore, the pore structures of the prepared alumina were mainly formed during the spray pyrolysis process.

Table 1. Specific Surface Areas and Pore Structures (Volume and Size) of Obtained Alumina and Different Precursors [Alumisol, $AlCl_3$, and $Al(NO_3)_3$]

	S_{BET} (m^2·g^{-1})	V_{BJH} (cm^3·g^{-1})	D_{BJH} (nm)
$Al_2O_{3\text{-sol}}$	284.5	0.3597	4.314
$Al_2O_{3\text{-AlCl3}}$	69.16	0.1884	4.269
$Al_2O_{3\text{-Al(NO3)3}}$	5.803	0.0435	3.332
alumisol	359.1	0.3247	3.560
$AlCl_3·6H_2O$	0.04604	0.0004457	1.412
$Al(NO_3)_3·9H_2O$	2.397	0.02415	12.41

3.3. Morphologies of Prepared Alumina and Precursors. The morphologies of the prepared alumina particles

dx.doi.org/10.1021/ie401243p | Ind. Eng. Chem. Res. 2013, 52, 13377−13383

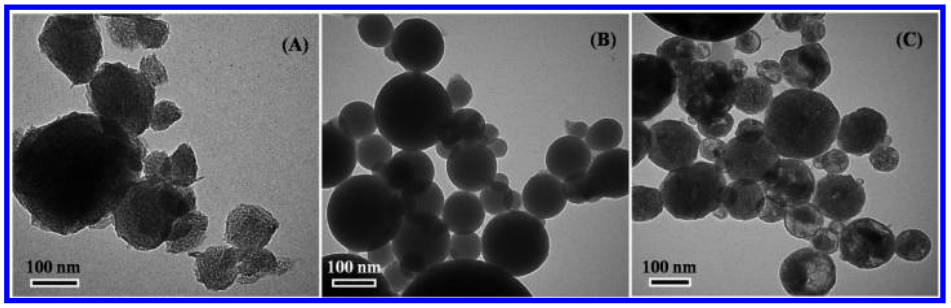

Figure 4. TEM micrographs of alumina particles prepared from (A) alumisol, (B) $Al(NO_3)_3$, and (C) $AlCl_3$ at 1000 °C with a carrier air flow rate of 1.0 L·min^{-1}.

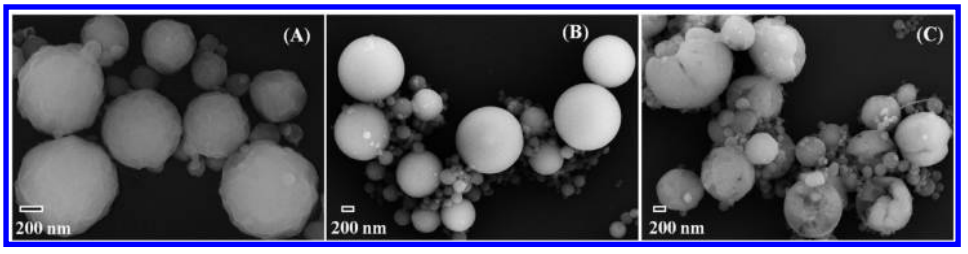

Figure 5. SEM micrographs of alumina particles prepared from (A) alumisol, (B) $Al(NO_3)_3$, and (C) $AlCl_3$ at 1000 °C with a carrier air flow rate of 1.0 L·min^{-1}.

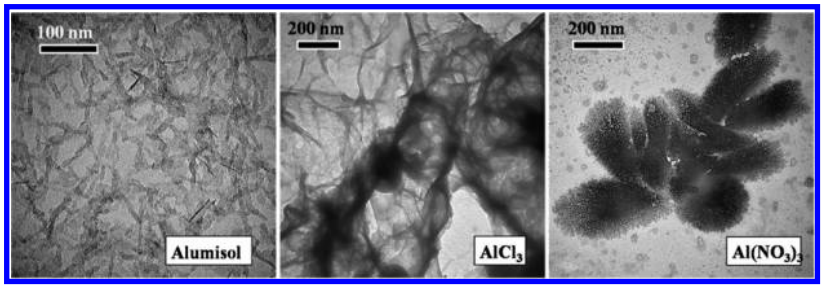

Figure 6. TEM micrographs of sprayed precursor droplets. (Samples were directly collected from the holders after atomization.)

was characterized by TEM and SEM measurements. Figures 4 and 5 clearly show that all of the particles had spherical shapes regardless of the precursors. Particles prepared from alumisol exhibited a rough surface (Figure 5A). The TEM micrograph (Figure 4A) showed that they presented an interconnected worm-like pore network, in good accordance with the N_2 adsorption−desorption analysis result. Particles prepared from $Al(NO_3)_3$ exhibited a uniform spherical-shaped morphology and a quite smooth surface, as shown by both TEM (Figure 4B) and SEM (Figure 5B). The homogeneity of the particles presented by TEM implied that these particles were solid and dense, in agreement with the results derived from BET measurement (Figure 3A). The highly spherical shape, quite smooth surface, and homogeneity of the obtained solid particles suggested that the atomized $Al(NO_3)_3$ droplets underwent melting during the pyrolysis process. The morphology of the alumina particles prepared from $AlCl_3$ showed a slight difference between the SEM and TEM micrographs. The SEM micrograph (Figure 5C) showed that particles with diameters of less than about 500 nm were spherical whereas particles larger than 500 nm split open. Meanwhile, in the TEM micrograph (Figure 4C), the particles maintained a spherical shape because only small particles smaller than about 400 nm could be characterized by TEM. Combined with the BET results (Figure 3A), the inhomogeneous brightness sheets in the TEM micrograph can be attributed to the lamellar structure instead of fragments of broken particles.

The nonuniform spherical shape of the particles prepared by the spray route is related to several factors such as the drying rate,[46,47] the volume fraction of colloids in the droplets,[32] and the rate of solute diffusion.[25] For example, when the rate of solute diffusion is much higher than that of solvent evaporation, hollow or even fragmented particles are often formed in addition to solid and spherical particles.[25] All of these factors might contribute to the formation of fissured particles prepared from $AlCl_3$ in the present work. In addition, the lamellar pores of particles might also lead to a fragile structure and conduce to the slitting of the obtained particles. Both solid particles and porous particles with an interconnected worm-like pore network are less fragile than particles with a lamellar structure. This result also implies that the stability of the morphology is related to the pore structure.

The precursor droplets were also characterized by TEM measurements. Atomized droplets were directly collected onto the sample holders (Cu grids) and allowed to dry. As shown in Figure 6, the suspended colloidal particles (AlOOH) in alumisol droplets were found to be rod-shaped with a width of 2−3 nm and a length of 20 nm. We have proposed that these colloidal rods cross-linked with each other to form the pore structure framework in the atomized alumisol droplets and that further evaporation of water through the interspaces of the

dx.doi.org/10.1021/ie401243p | Ind. Eng. Chem. Res. 2013, 52, 13377−13383

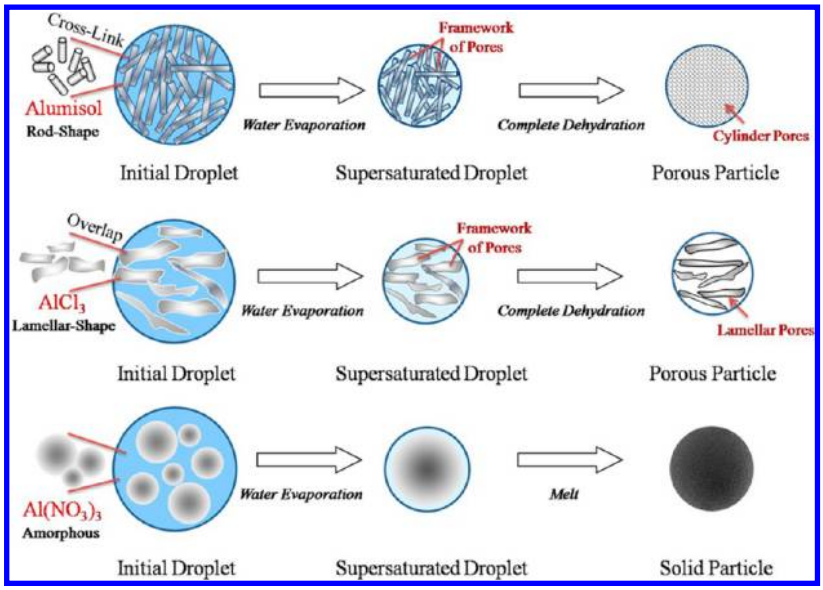

Figure 7. Possible formation mechanism of pore structures of alumina particles prepared from different precursors.

framework led to the formation of pores.[36] This implies that there is close relationship between the precursor morphology and the microstructure of the product. Indeed, in the case of the $AlCl_3$ precursor, the morphology was examined to be floccus-like and lamellar-shaped. It should be noticed that $AlCl_3$ hydrolyzes in water to produce HCl and flocculent precipitate of $Al(OH)_3$. However, because $AlCl_3$ could not hydrolyze completely, the component of the lamellar-shaped structure was therefore a mixture of $Al(OH)_3$ and $AlCl_3$. It is likely that the overlap of the mixture flakes gave rise to the frameworks of porous structure with lamellar pores. Meanwhile, the $Al(NO_3)_3$ precursor was characterized to be amorphous without a uniform shape, and the alumina prepared from $Al(NO_3)_3$ exhibited a uniform spherical-shaped morphology. It seems that the porosity of the prepared alumina was independent of the morphology of the $Al(NO_3)_3$ precursor. It has been proposed that, during the flame spray pyrolysis process, $Al(NO_3)_3$ precursor appears to melt during decomposition rather than volatilize.[48,49] Unlike $AlCl_3$, $Al(NO_3)_3$ does not hydrolyze in water, and aluminum hydrates hardly form in the solution. Therefore, the atomized $Al(NO_3)_3$ droplets might undergo melting during the spray pyrolysis process and finally form solid particles.

3.4. Possible Formation Mechanism of Different Pore Structures. The spray pyrolysis process generally involves four major steps:[19,25] generation of droplets from precursor solution, shrinkage of droplet size due to evaporation, conversion of the precursor into oxides, and formation of product particles. The generation of porosity has been demonstrated to be attributed to the evaporation of solvent from the interspaces of porous frameworks. For example, Tsai et al.[50] indicated that the formation of porous particles is due to a high solvent evaporation rate.

In this study, water was used as the solvent in precursor solutions. When the atomized precursor droplets went through the diffusion dryer, water partly evaporated, leading to the formation of supersaturated droplets having a preliminary framework of pore structures (as shown by Figure 7). The porous frameworks were found to be closely related to the morphologies of the precursors. The colloidal particles in alumisol are rod-shaped. During atomization, the colloidal rods cross-linked with each other to form the framework of the pore structure. Further evaporation of water through the interspaces of the framework resulted in the formation of cylindrical pore networks. The morphology of $AlCl_3$ crystal was characterized to be lamellar-shaped by TEM. The flakes of $AlCl_3$ crystals [perhaps mixed with $Al(OH)_3$ as a result of hydrolyzation] overlapped in the supersaturated droplets, and water and HCl (formed during the hydrolyzation) evaporated through the slits of the porous frameworks, resulting in the formation of lamellar pores. Although the final particles obtained from $Al(NO_3)_3$ were solid, water evaporation might also result in the formation of a porous framework in the supersaturated droplets. After the water evaporation process, the supersaturated droplets completely dehydrated during the pyrolysis process at high temperature (1000 °C). The particles obtained after complete dehydration were alumina particles. Evaporation of residual water through the interspaces of the porous frameworks led to the generation of cylindrical pore networks (for the alumisol precursor) or a lamellar pore structure (for the $AlCl_3$ precursor). For particles obtained from $Al(NO_3)_3$, the small specific surface area (5.803 $m^2 \cdot g^{-1}$) and pore volume (0.0435 $cm^3 \cdot g^{-1}$), as well as the highly spherical shape and the extremely smooth surface, imply that the amorphous precursor undergoes melting during the pyrolysis process, forming solid particles instead of porous particles.

4. CONCLUSIONS

γ-Al_2O_3 samples with different pore structures were prepared from alumisol, $AlCl_3 \cdot 6H_2O$, and $Al(NO_3)_3 \cdot 9H_2O$ by the spray pyrolysis method. Mesoporous alumina materials with quite narrow pore size distributions were generated from the alumisol and $AlCl_3$ precursors, whereas solid alumina particles were produced from the $Al(NO_3)_3$ precursor. The morphologies of the precursors were considered to be the critical factor in the formation of various pore structures. The rod-shaped colloidal particles in the alumisol cross-linked with each other to form a mesoporous framework with cylindrical pores. Lamellar-shaped $AlCl_3$ [mixed with $Al(OH)_3$] flakes overlapped during atomization and evaporation and led to the formation of lamellar pores. $Al(NO_3)_3$ underwent melting during its decomposition, resulting in the generation of solid particles.

AUTHOR INFORMATION

Corresponding Author

*Tel.: +86 10 62849123. Fax: +86 10 62923563. E-mail: honghe@rcees.ac.cn.

Notes

The authors declare no competing financial interest.

ACKNOWLEDGMENTS

This research was financially supported by the National Natural Science Foundation of China (20937004, 41305116, and 21107129). The authors gratefully appreciate the kind help of Professor Jinian Shu in the design of the atomizer.

REFERENCES

(1) Čejka, J. Organized Mesoporous Alumina: Synthesis, Structure and Potential in Catalysis. *Appl. Catal. A* **2003**, *254*, 327.

(2) He, H.; Zhang, X. L.; Wu, Q.; Zhang, C. B.; Yu, Y. B. Review of Ag/Al_2O_3-Reductant System in the Selective Catalytic Reduction of NOx. *Catal. Surv. Asia* **2008**, *12*, 38.

(3) Nassar, N. N.; Hassan, A.; Pereira-Almao, P. Effect of Surface Acidity and Basicity of Aluminas on Asphaltene Adsorption and Oxidation. *J. Colloid Interface Sci.* **2011**, *360*, 233.

(4) Martín, M. I.; Rabanal, M. E.; Gomez, L. S.; Torralba, J. M.; Milosevic, O. Microstructural and Morphological Analysis of Nanostructured Alumina Particles Synthesized at Low Temperature via Aerosol Route. *J. Eur. Ceram. Soc.* **2008**, *28*, 2487.

(5) Du, T.-B.; Jang, S.-M.; Chen, B.-W. Manufacture of Mesoporous Alumina of Boehmite Type via Subcritical Drying and Application to Purify Liquid Crystal. *Chem. Eng. Sci.* **2007**, *62*, 4864.

(6) Han, C. Y.; Li, H. Y.; Pu, H. P.; Yu, H.; Deng, L.; Huang, L. S.; Luo, Y. Synthesis and Characterization of Mesoporous Alumina and Their Performances for Removing Arsenic(V). *Chem. Eng. J.* **2013**, *217*, 1.

(7) Ghosh, S.; Naskar, M. K. Synthesis of Mesoporous γ-Alumina Nanorod Using a Double Surfactant System by Reverse Microemulsion Process. *RSC Adv.* **2013**, *3*, 4207.

(8) Song, K. C.; Kim, J. H.; Jung, K. Y.; Park, Y. K.; Jeon, J. K. Preparation of Mesoporous Alumina Particles by Spray Pyrolysis and Application to Double Bond Migration of 2-Butene. *J. Nanosci. Nanotechnol.* **2011**, *11*, 6312.

(9) Zhu, Z.; Liu, H.; Sun, H.; Yang, D. Surfactant Assisted Hydrothermal and Thermal Decomposition Synthesis of Alumina Microfibers with Mesoporous Structure. *Chem. Eng. J.* **2009**, *155*, 925.

(10) Koh, J.; Lee, J.; Kim, H.; Cho, A.; Moon, S. Correlation of the Deactivation of $CoMo/Al_2O_3$ in Hydrodesulfurization with Surface Carbon Species. *Appl. Catal. B* **2009**, *86*, 176.

(11) Borgna, A.; Garetto, T. F.; Apesteguía, C. R. Simultaneous Deactivation by Coke and Sulfur of Bimetallic Pt−Re(Ge, Sn)/Al_2O_3 Catalysts for *n*-Hexane Reforming. *Appl. Catal. A* **2000**, *197*, 11.

(12) Aguado, J.; Escola, J.; Castro, M.; Paredes, B. Metathesis of 1-Hexene over Rhenium Oxide Supported on Ordered Mesoporous Aluminas: Comparison with Re_2O_7/γ-Al_2O_3. *Appl. Catal. A* **2005**, *284*, 47.

(13) Ertl, G.; Knözinger, H.; Weitkamp, J. *Preparation of Solid Catalysts*; Willey-VCH Verlag Gmbh: Berlin, 1999.

(14) Komarneni, S. Some Significant Advances in Sol-gel Processing of Dense Structural Ceramics. *J. Sol−Gel Sci. Technol.* **1996**, *6*, 127.

(15) Xiao, F. S.; Qiu, S.; Pang, W.; Xu, R. New Developments in Microporous Materials. *Adv. Mater.* **1999**, *11*, 1091.

(16) Pratsinis, S. Flame Aerosol Synthesis of Ceramic Powders. *Prog. Energy Combust. Sci.* **1998**, *24*, 197.

(17) Tani, T.; Takatori, K.; Pratsinis, S. Dynamics of Hollow and Solid Alumina Particle Formation in Spray Flames. *J. Am. Ceram. Soc.* **2004**, *87*, 523.

(18) Manivasakan, P.; Karthik, A.; Rajendran, V. Mass Production of Al_2O_3 and ZrO_2 Nanoparticles by Hot-Air Spray Pyrolysis. *Powder Technol.* **2013**, *234*, 84.

(19) Gurav, A.; Kodas, T.; Pluym, T.; Xiong, Y. Aerosol Processing of Materials. *Aerosol. Sci. Tech.* **1993**, *19*, 411.

(20) Li, C. Z.; Hu, Y. J.; Yuan, W. K. Nanomaterials Synthesized by Gas Combustion Flames: Morphology and Structure. *Particuology* **2010**, *8*, 556.

(21) Mooney, J. B.; Radding, S. B. Spray Pyrolysis Processing. *Annu. Rev. Mater. Sci.* **1982**, *12*, 81.

(22) Rudin, T.; Pratsinis, S. E. Homogeneous Iron Phosphate Nanoparticles by Combustion of Sprays. *Ind. Eng. Chem. Res.* **2012**, *51*, 7891.

(23) Strobel, R.; Alfons, A.; Pratsinis, S. Aerosol Flame Synthesis of Catalysts. *Adv. Powder Technol.* **2006**, *17*, 457.

(24) Mueller, R.; Madler, L.; Pratsinis, S. E. Nanoparticle Synthesis at High Production Rates by Flame Spray Pyrolysis. *Chem. Eng. Sci.* **2003**, *58*, 1969.

(25) Okuyama, K.; Wuled Lenggoro, I. Preparation of Nanoparticles via Spray Route. *Chem. Eng. Sci.* **2003**, *58*, 537.

(26) Widiyastuti, W.; Balgis, R.; Iskandar, F.; Okuyama, K. Nanoparticle Formation in Spray Pyrolysis under Low-Pressure Conditions. *Chem. Eng. Sci.* **2010**, *65*, 1846.

(27) Rosner, D. E. Flame Synthesis of Valuable Nanoparticles: Recent Progress/Current Needs in Areas of Rate Laws, Population Dynamics, and Characterization. *Ind. Eng. Chem. Res.* **2005**, *44*, 6045.

(28) Aruna, S. T.; Balaji, N.; Shedthi, J.; Grips, V. K. Effect of Critical Plasma Spray Parameters on the Microstructure, Microhardness and Wear and Corrosion Resistance of Plasma Sprayed Alumina Coatings. *Surf. Coat. Technol.* **2012**, *208*, 92.

(29) Santos Abreu, A.; Knoll, M.; Moosburger-Will, J.; Konrad, A.; Tidecks, R.; Horn, S. Alumina and Yttria Powder and Yttria Coatings Made by Ultrasonic Spray Pyrolysis. *Chem. Vap. Deposition* **2013**, *19*, 15.

(30) Martín, M. I.; Gómez, L. S.; Milosevic, O.; Rabanal, M. E. Nanostructured Alumina Particles Synthesized by the Spray Pyrolysis Method: Microstructural and Morphological Analyses. *Ceram. Int.* **2010**, *36*, 767.

(31) Kim, S.; Liu, B.; Zachariah, M. Synthesis of Nanoporous Metal Oxide Particles by a New Inorganic Matrix Spray Pyrolysis Method. *Chem. Mater.* **2002**, *14*, 2889.

(32) Sen, D.; Mazumder, S.; Melo, J.; Khan, A.; Bhattyacharya, S.; D'Souza, S. Evaporation Driven Self-Assembly of a Colloidal Dispersion during Spray Drying: Volume Fraction Dependent Morphological Transition. *Langmuir* **2009**, *25*, 6690.

(33) Hu, Y.; Li, C. Z.; Gu, F.; Ma, J. Preparation and Formation Mechanism of Alumina Hollow Nanospheres via High-Speed Jet Flame Combustion. *Ind. Eng. Chem. Res.* **2007**, *46*, 8004.

(34) Hu, Y. J.; Ding, H. Q.; Li, C. Z. Preparation of Hollow Alumina Nanospheres via Surfactant-Assisted Flame Spray Pyrolysis. *Particuology* **2011**, *9*, 528.

(35) Kim, J.; Jung, K.; Park, K.; Cho, S. Characterization of Mesoporous Alumina Particles Prepared by Spray Pyrolysis of $Al(NO_3)_2{\cdot}9H_2O$ Precursor: Effect of CTAB and Urea. *Microporous Mesoporous Mater.* **2010**, *128*, 85.

(36) Liu, C.; Liu, Y. C.; Ma, Q. X.; He, H. Mesoporous Transition Alumina with Uniform Pore Structure Synthesized by Alumisol Spray Pyrolysis. *Chem. Eng. J.* **2010**, *163*, 133.

(37) Boissière, C.; Nicole, L.; Gervais, C.; Babonneau, F.; Antonietti, M.; Amenitsch, H.; Sanchez, C.; Grosso, D. Nanocrystalline Mesoporous γ-Alumina Powders "UPMC1 Material" Gathers Thermal and Chemical Stability with High Surface Area. *Chem. Mater.* **2006**, *18*, 5238.

(38) Santos, P.; Santos, H.; Toledo, S. Standard Transition Aluminas. Electron Microscopy Studies. *Mater. Res.* **2000**, *3*, 104.

(39) Chatterjee, M.; Enkhtuvshin, D.; Siladitya, B.; Ganguli, D. Hollow Alumina Microspheres from Boehmite Sols. *J. Mater. Sci.* **1998**, *33*, 4937.

(40) Wang, W.; Lenggoro, I.; Okuyama, K. Dispersion and Aggregation of Nanoparticles Derived from Colloidal Droplets under Low-Pressure Conditions. *J. Colloid Interface Sci.* **2005**, *288*, 423.

(41) Maskara, A.; Smith, D. M. Agglomeration during the Drying of Fine Silica Powders, Part II: The Role of Particle Solubility. *J. Am. Ceram. Soc.* **1997**, *80*, 1715.
(42) Klobes, P.; Meyer, K.; Munro, R. G. *Porosity and Specific Surface Area Measurements for Solid Materials*; NIST Special Publication 960-17; National Institute of Standards and Technology: Gaithersburg, MD, 2006.
(43) Sing, K. S. W.; Everett, D. H.; Haul, R. A. W.; Moscou, L.; Piepotti, R. A.; Rouquerol, J.; Siemieniewska, T. Reporting Phyisorption Data for Gas Solid Systems with Special Reference to the Determination of Surface Area and Porosity. *Pure Appl. Chem.* **1985**, *57*, 603.
(44) Vaudry, F.; Khodabandeh, S.; Davis, M. Synthesis of Pure Alumina Mesoporous Materials. *Chem. Mater.* **1996**, *8*, 1451.
(45) Chen, F.; Meng, X.; Xiao, F. S. Mesoporous Solid Acid Catalysts. *Catal. Surv. Asia* **2011**, *15*, 37.
(46) Tsapis, N.; Dufresne, E. R.; Sinha, S. S.; Riera, C. S.; Hutchinson, J. W.; Mahadevan, L.; Weitz, D. A. Onset of Buckling in Drying Droplets of Colloidal Suspensions. *Phys. Rev. Lett.* **2005**, *94*, 018302.
(47) Iskandar, F.; Gradon, L.; Okuyama, K. Control of the Morphology of Nanostructured Particles Prepared by the Spray Drying of a Nanoparticle Sol. *J. Colloid Interface Sci.* **2003**, *265*, 296.
(48) Hinklin, T.; Toury, B.; Gervais, C.; Babonneau, F.; Gislason, J.; Morton, R.; Laine, R. Liquid-Feed Flame Spray Pyrolysis of Metalloorganic and Inorganic Alumina Sources in the Production of Nanoalumina Powders. *Chem. Mater.* **2004**, *16*, 21.
(49) Messing, G.; Zhang, S.; Jayanthi, G. Ceramic Powder Synthesis by Spray Pyrolysis. *J. Am. Ceram. Soc.* **1993**, *76*, 2707.
(50) Tsai, S.; Song, Y.; Tsai, C.; Yang, C.; Chiu, W.; Lin, H. Ultrasonic Spray Pyrolysis for Nanoparticles Synthesis. *J. Mater. Sci.* **2004**, *39*, 3647.